Physica A 455 (2016) 79–91

Contents lists available at ScienceDirect

Physica A

journal homepage: www.elsevier.com/locate/physa

# Effects of vascularization on cancer nanochemotherapy outcomes

L.R. Paiva [a], S.C. Ferreira [b], M.L. Martins [b,c,*]

[a] Departamento de Física e Matemática, Universidade Federal de São João Del-Rei, Campus Alto Paraopeba, 36420-000, Ouro Branco, Minas Gerais, Brazil

[b] Departamento de Física, Universidade Federal de Viçosa, 36570-000, Viçosa, MG, Brazil

[c] National Institute of Science and Technology for Complex Systems, Centro Brasileiro de Pesquisas Físicas, Rua Xavier Sigaud 150, 22290-180, Rio de Janeiro, Brazil

## HIGHLIGHTS

- A 3D model for chemotherapy based on anticancer nanoparticles is investigated.
- Therapeutic success is mainly determined by the nanoparticle endocytic rate.
- The eradication of highly vascularized tumors demands more aggressive therapies.
- Our results discourage the use of therapies that normalize the tumor vasculature.

## ARTICLE INFO

*Article history:*
Received 5 August 2015
Received in revised form 11 January 2016
Available online 7 March 2016

*Keywords:*
Cancer
Nanochemotherapy
Tumoral vasculature
Multiscale modeling

## ABSTRACT

Cancer therapy requires anticancer agents capable of efficient and uniform systemic delivery. One promising route to their development is nanotechnology. Here, a previous model for cancer chemotherapy based on a nanosized drug carrier (Paiva et al., 2011) is extended by including tissue vasculature and a three-dimensional growth. We study through computer simulations the therapy against tumors demanding either large or small nutrient supplies growing under different levels of tissue vascularization. Our results indicate that highly vascularized tumors demand more aggressive therapies (larger injected doses administrated at short intervals) than poorly vascularized ones. Furthermore, nanoparticle endocytic rate by tumor cells, not its selectivity, is the major factor that determines the therapeutic success. Finally, our finds indicate that therapies combining cytotoxic agents with antiangiogenic drugs that reduce the abnormal tumor vasculature, instead of angiogenic drugs that normalize it, can lead to successful treatments using feasible endocytic rates and administration intervals.



## 1. Introduction

Cancer, owing to its metastatic spreading through the organism, requires therapies based on medicines capable of efficient and uniform systemic delivery. Conventional chemotherapeutic agents exhibit several limitations such as nonspecific biodistribution and targeting, toxicity and low therapeutic indices [1]. Packaging clinically approved drugs into nanoscale delivery vehicles is a promising strategy for developing safe and efficacious anticancer treatments [2].

* Corresponding author at: Departamento de Física, Universidade Federal de Viçosa, 36570-000, Viçosa, MG, Brazil.
*E-mail address:* mmartins@ufv.br (M.L. Martins).

http://dx.doi.org/10.1016/j.physa.2016.02.065
0378-4371/

Nanoparticles, in order to achieve passive targeting to tumors via the enhanced permeability and retention effects, should be large enough in size to prevent their rapid leakage from normal capillaries but functionalized and small enough to avoid opsonization in the blood and rapid clearing by the reticulo-endothelial system in liver, lungs, spleen, and bone marrow. Consequently, the size of nanoparticles should be up to 100 nm to reach tumor affected tissues [3]. According to Perrault et al. [4], studying the effect of nanoparticle size on tumor accumulation in a murine cancer model, the optimal nanoparticle size is approximately 60–80 nm. In addition to size, nanoparticles should ideally have a hydrophilic surface to escape macrophage capture [3]. Also, as positive-charged nanoparticles lead to significant immune reactions, neutral and negatively charged ones are preferable for clinical application [1].

Simultaneously to the quest for therapeutic agents with optimal physicochemical properties, other strategies to overcome drug delivery barriers exploring the repair of the tumor abnormal physiology are in progress [5]. These alternatives include as a target the tumor vasculature. If the abnormal structure and function of the tumor vascular network can be transiently normalized by some angiogenic drugs, more efficient oxygen and drug delivery is provided, alleviating hypoxia and increasing therapeutic efficacy [6–8]. Improving blood flow in tumors also means enhancing the nutrient supply to cancer cells. Thus, although remaining in the proof-of-principle stage, this approach apparently underestimates the latter effect, antagonic to the former one. At the theoretical level, mathematical models can provide valuable insights about the efficacy of combined therapies based on antiangiogenic agents that normalize the abnormal tumor vasculature and cytotoxic drugs.

Angiogenesis, vascular remodeling, tumor blood perfusion, drug accumulation in cancerous vasculature, interstitial flow, and cellular drug response are major features in cancer chemotherapy. From the recent literature we can highlight several mathematical models focused on the understanding of each one of these features (for instance, Refs. [9,10] for angiogenesis and vascular adaptation; [11–13] for blood perfusion and interstitial flow; [14–16] for drug delivery and [17] for cellular response). In particular, regarding vascularization and interstitial flow, these models reveal that (i) the collapse and regression of vessels accelerates perfusion and all portions of the remodeled tumor vasculature are reached by a tracer substance flowing through the network [11]. Consequently, (ii) the interstitial flow emerges as the key component of the drug delivery barrier [12]. Indeed, the interstitial pressure inside the tumor is uniformly high and abruptly decreases at the periphery, generating a very slow interstitial flow within the tumor and a rapidly rising convective flow outwards the tumor. In addition, an elevated interstitial hydraulic conductivity together with poor lymphatic drainage causes the plateau profile of the interstitial fluid pressure and contributes to a broad-based collapse of the tumor lymphatics [13]. Naturally, these and other models inspired or evolved to multiscale approaches integrating most of those major features involved in cancer chemotherapy [18,19].

Here, we address the *in silico* cancer therapy based on chimeric polypeptides (CP) that self-assemble into nanoparticles on doxorubicin (Dox) attachment [20]. These drug-loaded nanoparticles display good pharmacokinectics and tumor accumulation, low toxicity and high antitumoral efficacy. Specifically, we investigate via computer simulations the effects of pre-existent tissue vasculature, CP–Dox nanoparticle endocytic rate and selectivity for cancer cells, therapeutic doses and administration intervals on the treatment outcomes. The model assumes a 3D vasculature network which supplies nutrients and nanomedicines to the tumor affected tissue. After extravasating the capillaries, these chemicals are transported through the interstitium mainly by diffusion and uptake by cells. Inside the cells, doxorubicin released from the CP–Dox nanoparticles disassemble impaired cell viability, eventually eliciting cell death. The pharmacokinetics of CP–Dox nanoparticles is accounted in an effective, empirical manner, thus neglecting detailed molecular interaction mechanisms. Similarly, cell responses to their microenvironment are translated into stochastic actions (proliferation and death) regulated by local concentrations of nutrients and drugs supplied by the tissue vasculature. Finally, the spatio-temporal concentration distributions of nutrients and drugs are determined by the vasculature geometry. Besides more realistic, a 3D geometry for the vasculature and its surrounding tissue enables a richer set of reaction–diffusion growth patterns than in 2D systems [21–23]. A paramount biological illustration of this precept is heart arrhythmias. Ventricular fibrillation is a three-dimensional phenomena, i.e., that only occurs in sufficiently thick heart muscle [24].

The outline of this paper is as follows. In Section 2, the model is described. It extends our previous models introduced in Refs. [21,23] by introducing a three-dimensional tissue fed through a vascular network. As before, the model considers cells as individual agents whereas nutrients, CP–Dox nanoparticles and free Dox are continuous fields. The simulation results are reported in Section 3 and discussed in Section 4. Finally, our conclusions are drawn in Section 5. Appendices A and B present complementary details of the model.

## 2. The model

The model consists of a cubic lattice (the tissue) fed by a capillary vessel network established before the emergence of the first cancer cell and that does not evolve in time. Their capillaries branch throughout the normal tissue according to correlated random walks starting from randomly chosen sites on either the bottom or lateral lattice borders. Specifically, each vessel proceeds in a randomly chosen direction (defined by the axial and azimuthal angles $\phi$ and $\theta$) with fixed perturbations $\delta\phi$, $\delta\theta$. Further details about the capillary network model are presented in Appendix A.

Sites associated to the capillary network cannot be occupied by either normal or cancer cells. Any site that does not belong to the capillary network can be occupied by normal or cancer cells. These cells are individual agents and their populations

$\sigma_n(\vec{x})$ and $\sigma_c(\vec{x})$, respectively, obey the constraint $\sigma_n(\vec{x}) + \sigma_c(\vec{x}) \leq \sigma_{\max}$ at every site $\vec{x}$. Here, $\sigma_{\max}$ is the maximum number of cells supported by each site. The nutrient concentration is described by the diffusion equation

$$\frac{\partial \Phi(\vec{x}, t)}{\partial t} = D_N \nabla^2 \Phi(\vec{x}, t) - \beta' \Phi(\vec{x}, t)\sigma_n(\vec{x}, t) - \lambda_\Phi \beta' \Phi(\vec{x}, t)\sigma_c(\vec{x}, t), \tag{1}$$

in which $D_N$ is the nutrient's diffusivity, the nutrient absorption terms are proportional to the cell populations present in each site, and distinct nutrient uptake rates ($\beta'$ and $\lambda_\Phi \beta'$, respectively) for normal and cancer cells are assumed. By performing the variable transformations used in Ref. [21], Eq. (1) assumes the dimensionless form

$$\frac{\partial \Phi(\vec{x})}{\partial t} = \nabla^2 \Phi(\vec{x}) - \beta^2 \Phi(\vec{x})\sigma_n(\vec{x}) - \lambda_\Phi \beta^2 \Phi(\vec{x})\sigma_c(\vec{x}), \tag{2}$$

with a characteristic length scale $\beta = \Delta\sqrt{\beta'/D_N}$ (see Appendix B) for nutrient diffusion. Eq. (2) obeys periodic boundary conditions along the longitudinal borders of the tissue in the $xy$ plane and a Neumann (null flux) boundary condition at the $z$ direction. Biologically, $z = 0$ represents the insulating subcutaneous fatty tissue beneath the reticular dermis and $z = L$ the external border of the epithelial tissue. At the capillaries, the concentration is $\Phi = 1$ (fixed supply in proper unities).

The tumor grows, from a single malignant cell introduced at the central region of the lattice, according to stochastic dynamics involving cellular division and death. For sake of simplicity, normal cells do not divide. They only die due to drug cytotoxicity with a probability $P^n_{die}$,

$$P^n_{die} = \exp[-(V/\theta^n_{die})^2], \tag{3}$$

where $\theta^n_{die}$ controls the normal cell susceptibility to the drug and $V$ is an effective cell viability determined by the intracellular level $C_4(t)$ of released Dox, as defined below. The cell viability is determined by the pharmacokinetics of CP–Dox nanoparticles [20]. In the absence of therapy, $V = 1$ for all normal and cancer cells.

Cancer cells can divide or die with probabilities dependent on both the local nutrient concentration per cell and the effective cell viability $V$. Specifically, division and death probabilities are respectively given by

$$P^c_{div} = 1 - \exp\{-[V\Phi(\vec{x}, t)/(\sigma_c \theta^c_{div})]^2\}, \tag{4}$$

$$P^c_{die} = \exp\{-[V\Phi(\vec{x}, t)/(\sigma_c \theta^c_{die})]^2\}. \tag{5}$$

Here $\theta^c_{div}$ and $\theta^c_{die}$ are model parameters. At each time step, $N_c$ cancer cells are chosen (where $N_c$ is the total number of cancer cells at the beginning of the time step) and each one tries to execute an action – division or death – with equal chance. Chosen the cell action, the corresponding probability is evaluated. When a cancer cell is chosen to divide, its daughter cell stays at the same site as her mother if $\sigma_c(\vec{x}) < \sigma_{\max}$; otherwise the neighbor sites are checked. If there are one or more neighbor sites that do not belong to the capillary network and for which $\sigma_c(\vec{x'}) < \sigma_{\max}$, one of them is randomly chosen and occupied by the daughter cell, otherwise the cell does not divide. If there are normal cells in the occupied site, one of them is removed ($\sigma_n(\vec{x'}) = \sigma_n(\vec{x'}) - 1$).

The chemotherapy begins when the tumor attains $N_0$ cells, and consists of periodic, systemic administrations of CP–Dox at a dose $C_0$. In the blood, the nanoparticles concentration evolves as

$$\frac{dC_1}{dt} = -k_1 C_1 + C_0 \delta(t - n\tau), \tag{6}$$

where $k_1 = k_{el} + k_2$ is the drug's removal rate due to both clearance from the systemic circulation ($k_{el}$) and accumulation in the tissue ($k_2$); $n = 0, 1, 2, \ldots$ and $\tau$ is the interval between administrations. The pharmacokinetic parameters for Dox delivery were estimated elsewhere [20]. CP–Dox nanoparticles leaking from the capillaries into the tissue diffuse as

$$\frac{\partial C_2(\vec{x}, t)}{\partial t} = D\nabla^2 C_2(\vec{x}, t) - [\alpha_n \sigma_n(\vec{x}, t) + \alpha_c \sigma_c(\vec{x}, t)]C_2(\vec{x}, t), \tag{7}$$

with diffusivity $D$ and endocytic rate $\alpha_n$ ($\alpha_c$) for normal (cancer) cells. These parameters were estimated similarly as in Ref. [23]. Neumann boundary conditions (null flux) are imposed at the tissue external border. At the capillaries, the concentration is $C_2(\vec{x}, t) = k_2 C_1(t)$, where $\vec{x}$ is a site belonging to the capillary network.

At constant rates, a fraction of the local nanoparticles concentration $C_2(\vec{x}, t)$ is endocytosed by cells at every occupied site. Also, the internalized nanoparticles degrade and release ∼68% of their drug load [20,23]. So, the nanoparticles concentration inside a cell $i$ (normal or cancerous) at the site $\vec{x}$, varies in time as

$$\frac{dC^{(i)}_3(\vec{x}, t)}{dt} = \alpha^{(i)}_{n,c} C_2(\vec{x}, t) - C^{(i)}_3(\vec{x}, t), \tag{8}$$

and changes the intracellular free Dox concentration, $C^{(i)}_4(\vec{x}, t)$, by

$$\frac{dC^{(i)}_4(\vec{x}, t)}{dt} = 0.68 C^{(i)}_3(\vec{x}, t). \tag{9}$$

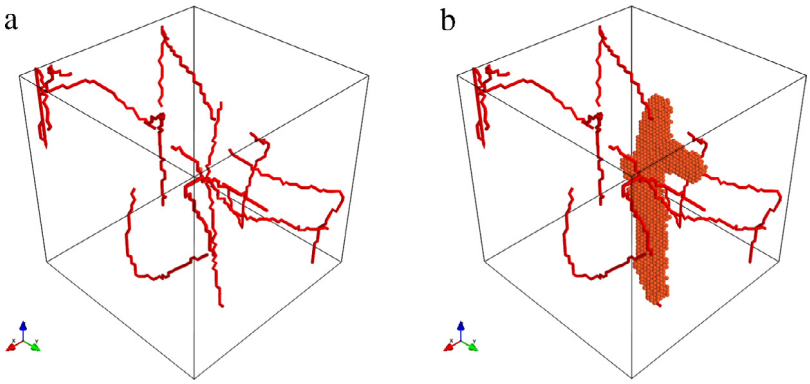


**Fig. 1.** (a) Typical vascular network and (b) an untreated tumor grown up to reach the lattice borders.

The free drug progressively impairs cell functions in a dose-dependent way. A cell "viability" function

$$V = 1/[1 + (C_4(t)/IC_{50})^p] \tag{10}$$

was used to model the Dox effect on cell actions. $IC_{50}$ and $p$ are parameters experimentally obtained by Mackay et al. [20].

Finally, as reported by Summers et al. [25], the partitioning of nanoparticles in cell division is random and asymmetric. So, upon cell division, the amounts of both internalized nanoparticles and free drug can be shared by mother and daughter cells. So, the model assumes that, every time a cancer cell divides, both their loads of nanoparticles (described by $C_3$) and free drug (described by $C_4$) are partitioned between the two resulting cells at the fractions $\omega$ and $1 - \omega$. Obviously, the therapy without partitioning of nanoparticles and free drug after cell division corresponds to $\omega = 0$ (or 1).

Although incorporating major traits of cancer growth and its chemotherapy, our model involves some simplifications. Indeed, concerning the vasculature, we assume a pre-existing and static vessel network instead of a dynamic one co-evolving with the growing tumor. A static vasculature, adequate for cutaneous melanoma [26,27], is less realistic for other solid tumors. Furthermore, since the model adopts fixed supply of nutrients by and constant rates of drug removal and transvascular flux at each vessel, the spatio-temporal variations of blood perfusion and nanoparticle accumulation in tumor vasculature are neglected. Hence, the simplest transport dynamics used in our model might correspond to an upper bound regime for real malignant neoplasias. Another simplification is the use of homogeneous diffusivities for nutrients and drug. In consequence, our model does not consider the plateau profile of the interstitial flow and, again, sets the system at an upper bound of drug delivery to cancer cells. Regarding drug transport into the cells, we simply adopt fixed cellular endocytic rates, independently on the phases of the cells in the cell-cycle, in contrast to experimental observations revealing that the dose of internalized nanoparticles varies as the cell advances through the cell-cycle [28]. Once again, this simplification contributes to maximize drug delivery.

## 3. Results

Simulations were performed in cubic tissue sections with linear size $L = 50\Delta = 1$ mm, where $\Delta$ is the lattice constant. Since it was assumed that the mean diameter of a cell is around 10 $\mu$m, the maximum number of cells in a lattice site is $\sigma_{\max} = 8$. The capillaries average $\sim$1 mm in length, as experimentally observed [29], and the parameters controlling the vessels tortuosity were chosen as $\delta\phi = 0.1$ and $\delta\theta = 0.2$ (Appendix A). The cancer cell parameters were fixed in $\lambda_\Phi = 10$, $\theta^c_{div} = 0.1$, $\theta^c_{die} = 0.001$ and for normal cells $\theta^n_{die} = 0.001$. The pharmacokinetic parameters associated to CP–Dox nanoparticles were taken from Ref. [20] and are those used in Ref. [23]. Finally, the simulation is stopped if a cancer cell reaches one of the tissue borders or after $10^4$ time steps (that corresponds to approximately 4.6 years). Further parameter values are reported in Appendix B.

### 3.1. Poorly vascularized tumors

The tumor grows in a tissue with a density of only 10 capillaries/mm$^3$, and their cells uptake nutrients at a high rate $\beta = 0.1$. Typical vascular networks, as the one shown in Fig. 1(a), yield average cell division and death probabilities, Eqs. (4) and (5), of $5.81 \times 10^{-3}$ and $2.6 \times 10^{-4}$, respectively.

In Fig. 1(b), a typical tumor is shown. It has $1.7 \times 10^4$ cells densely packaged in a mass containing very few empty spaces or normal cells. Since nutrients are scarce and uptake by cancer cells is high, the tumor grows slowly and constrained to the adjacencies of the capillary vessels, where the nutrient concentration is higher. Typically, the average nutrient concentration in the tissue, initially in 66% of the capillary concentration, decays to only 5.6% of its concentration in the capillaries at the end of the simulation. This limit value is consistent with observations that tumor glucose concentrations are frequently 3- to 10-fold lower than in non-transformed tissues [30,31]. Moreover, as the tumor grows, the nutrient concentration far

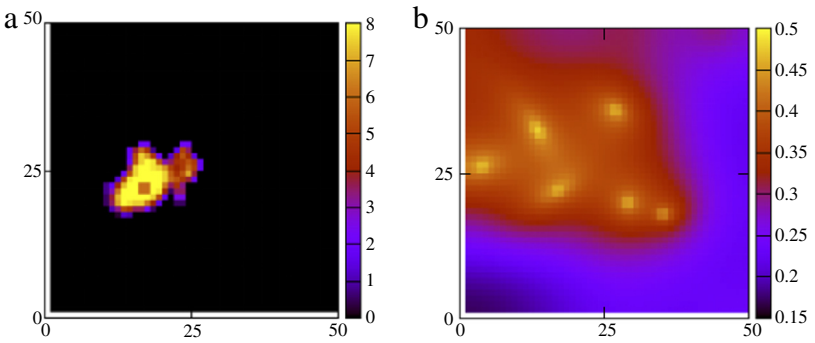


**Fig. 2.** Slices of (a) the poorly vascularized tumor and (b) the corresponding CP–Dox nanoparticles concentration at the center of the lattice immediately after the first round of a selective therapy with $\alpha_c = 1.0 \times 10^{-4}$ h$^{-1}$, $C_0 = 0.5$ mM and $\tau = 24$ h. The scale of colors in (a) refers to the number of cancer cells per site. The black region is occupied by the normal tissue. (For interpretation of the references to color in this figure legend, the reader is referred to the web version of this article.)

from the capillaries reaches values as low as 0.04% of the blood concentration in some regions. This fact together with the static nature of the vessel network is the root cause of tumor growth adjacent to the capillaries. In the absence of directed development of new vessels, the tumor grows by co-opting the vascular plexus present in the affected tissue, as observed in cutaneous melanoma [26,27].

*3.1.1. Therapies based on selective nanoparticles*

The nanoparticles are assumed perfectly selective for tumor cells, hence $\alpha_n = 0$, and there is no partitioning of CP–Dox ($\omega = 0$). Two nanoparticle endocytic rates by cancer cells were tested: $\alpha_c = 1.0 \times 10^{-4}$ (low) and $\alpha_c = 5.0 \times 10^{-3}$ h$^{-1}$ (high).

In Fig. 2 is shown a tumor slice taken at the middle of the lattice after the first dose $C_0 = 0.5$ mM of CP–Dox. Fig. 2(a) reveals that the tumor grows around a capillary vessel and that the cancer cell density decays fast with the distance from this capillary. Since the tumors grow around the capillary networks, necrotic cores were not observed in our simulations. Fig. 2(b) shows that the nanoparticles concentration is 0.5 mM at the regions occupied by capillary vessels and falls with the distance from the capillaries, but it is not significantly reduced into the region occupied by the tumor because the nanoparticle endocytic rate by tumor cells is low ($\alpha_c = 1.0 \times 10^{-4}$ h$^{-1}$).

For low $\alpha_c$, the tumor was not eradicated by the treatment even administrating the maximum tolerated dose of CP–Dox ($C_0 = 0.6$ mM) at each 4 h (see Figs. 3(a) and 4(c)). Aggressive therapies (doses $\geq 0.5$ mM administrated at short intervals of 4 h) are only able to shrink the tumor mass to a few thousand cells, as shown in Fig. 3(a). Further, such higher doses can abrogate the tumor exponential growth if administrated at 24 h intervals. Longer periods and lower doses, as for instance $C_0 = 0.2$ mM administrated at each 8 days, cannot block tumor growth as shown in Figs. 3(a) and 4(b). Summarizing, for low CP–Dox endocytic rates the tumor is not eradicated. Even worse, as revealed by Fig. 4(a) and (b), an ineffective therapy eventually leads to a malignant neoplastic mass increased in size in comparison with its size at the beginning of the treatment. Indeed, the death of tumor cells elicited by the therapy releases more space and nutrients only for the surviving malignant cells that further divide and replace normal cells.

Nevertheless, for high $\alpha_c$ the tumor can be eradicated at long-term. For instance, with a dose $C_0 = 0.5$ mM administrated each 24 or 36 h, the cancer is extinct in 11 or 37 months, respectively. Also, the number of cancer cells is drastically reduced to 10% of its value at the therapy beginning after approximately two months, opening an opportunity for a surgical excision of the tumor or the introduction of other combined therapy. However, lower doses and/or longer administration periods cannot eradicate the tumor. At most, these therapies lead to either an almost complete tumor remission or abrogate its exponential growth. For instance, a dose $C_0 = 0.5$ mM administrated at intervals of 2 or 3 days promotes strong tumor shrinking, while a lower dose ($C_0 = 0.2$ mM) administrated at each 8 days arrests tumor growth. These results are illustrated in Fig. 3(b). Summarizing, for high endocytic rates the tumor can be either eradicated or controlled with higher or lower doses, respectively, administrated at longer intervals.

*3.1.2. Therapies based on non-selective nanoparticles*

Non-selective nanoparticles, as actually is the case of CP–Dox, can be internalized by both normal and cancer cells. In Fig. 5 are shown the therapeutic outcomes of poorly vascularized tumors using either selective ($\alpha_n = 0$) or non-selective nanoparticles ($\alpha_c = \alpha_n \neq 0$). It can be noticed that the outcomes are very similar. This can be understood if we notice that the nanoparticle concentration far from the capillaries is negligible and that the tumor cells occupy almost entirely the regions surrounding the capillaries. The normal cells affected by the therapy are those close to capillaries in tumor-free regions. Since the nanoparticle concentration decays exponentially with the distance from the capillary and the tumor grows surrounding these blood vessels, the amount of nanoparticles uptaken by normal cells is small in comparison to that uptaken by tumor cells. So, the therapy selectivity does not change significantly the therapeutic outcomes.

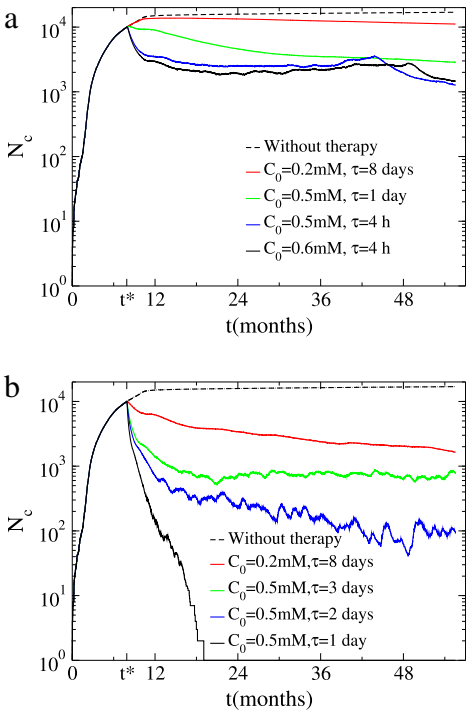


**Fig. 3.** Evolution of cancer cell population for a selective therapy against a poorly vascularized tumor with $\beta = 0.1$ for different administration protocols (injected doses $C_0$ and intervals $\tau$ between injections). Nanoparticles are absorbed only by cancer cells at rates (a) $\alpha_c = 1.0 \times 10^{-4}$ and (b) $\alpha_c = 5.0 \times 10^{-3}$ h$^{-1}$. Therapies begin at $t^*$.

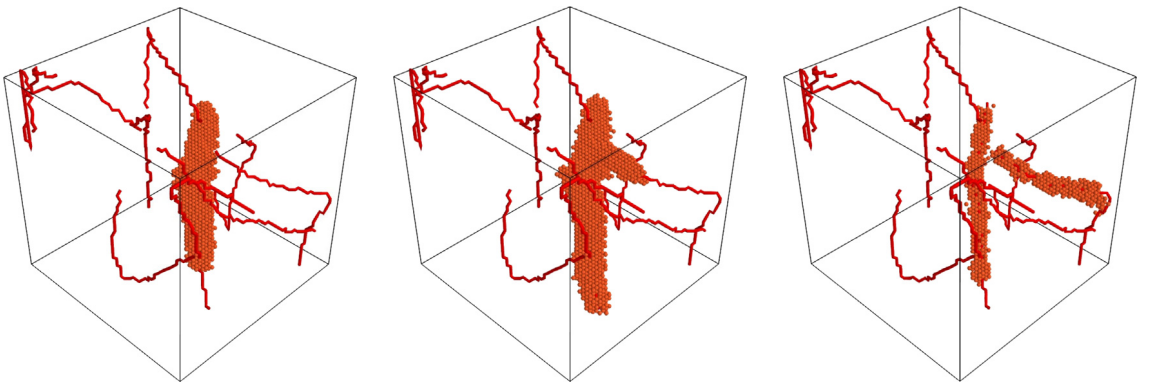

(a) Tumor just before the therapy.

(b) Tumor after therapy, $C_0 = 0.2$ mM, $\tau = 192$ h.

(c) Tumor after therapy, $C_0 = 0.6$ mM, $\tau = 4$ h.

**Fig. 4.** Poorly vascularized tumor ($\beta = 0.1$) and capillary network before (a) and after mild (b) and aggressive (c) selective therapies shown in Fig. 3 ($\alpha_c = 1.0 \times 10^{-4}$ h$^{-1}$). In these figures, each point represents a site occupied by at least one cancer cell, but the number of cells at each site is not represented. All these patterns were obtained for the last time step of the corresponding simulations ($t = 10^4 \sim 4.6$ y).

### 3.2. Highly vascularized tumors

In order to evaluate the role of the vascular network in tumor–drug dynamics, we also simulated the therapy against cancers fed by dense vasculatures (see Fig. 6(a)). Assuming the same nutrient uptake rate by cancer cells ($\beta = 0.1$), a larger nutrient availability is provided by twice capillary vessels. Under such conditions, the tumor grows faster sustaining significantly greater average cell division and smaller death probabilities ($1.5 \times 10^{-2}$ and $4.0 \times 10^{-5}$, respectively). Again, the highly vascularized tumor grows around the capillaries, but their cells, in an increased number ($2.2 \times 10^4$), extend deeper into the vessel surroundings, as shown in Fig. 6(b). Concerning the spatial nutrient distribution, the regions with minimum nutrient concentration are localized far from the capillaries and, consequently, distant from the tumor. Everywhere there are more nutrients available to the cells than throughout the poorly vascularized tumor previously considered (see for comparison Fig. 6(c) and (d)), as intuitively expected. The neoplastic growth perpendicular to the local capillary directions

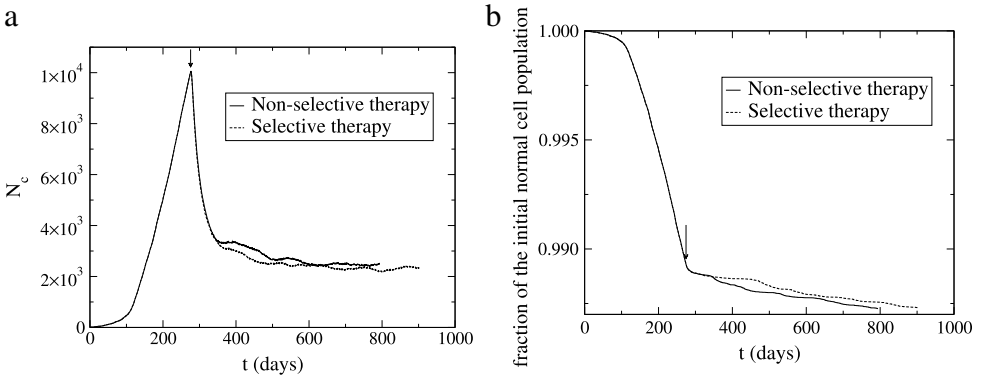


**Fig. 5.** Evolution in time of (a) cancer cell population and (b) fraction of survival normal cells for selective and non-selective therapies beginning at the instant indicated by the arrows ($t^*$).

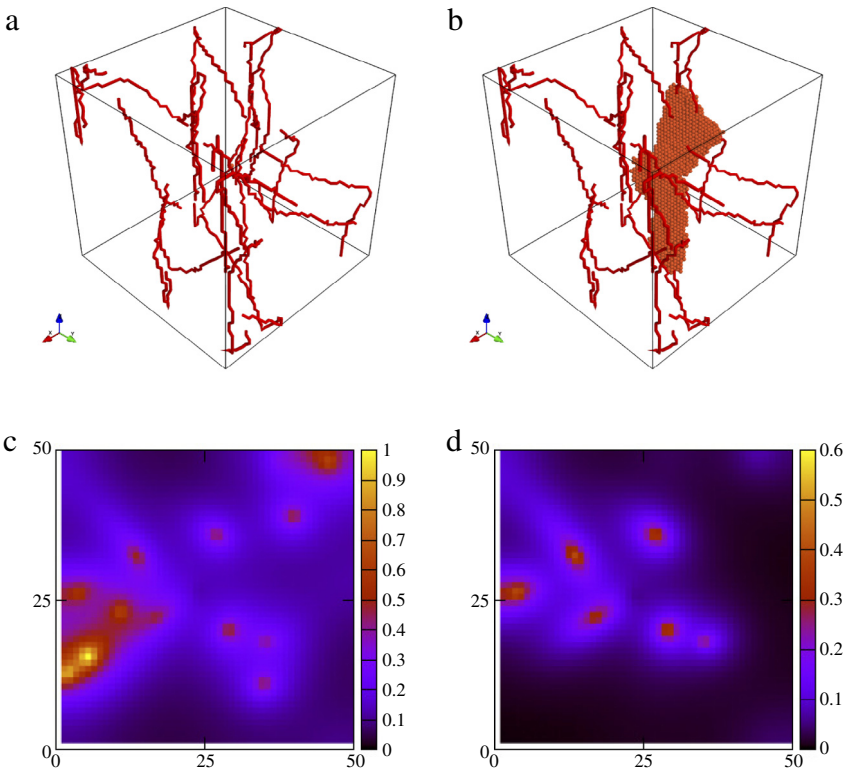


**Fig. 6.** (a) Typical dense capillary network with 20 capillaries/mm$^3$ and (b) a highly nutrient demanding tumor ($\beta = 0.1$) fed by this vasculature. (c) The spatial distribution of nutrients on a slice at the center of the lattice just before the therapy beginning. (d) The same nutrient concentration profile but for the poorly vascularized tumor of Fig. 1(b).

is enhanced by decreasing nutrient uptake rate (see Fig. 7(a)). Indeed, for $\beta = 0.08$, the average cell division probability increases further ($2.4 \times 10^{-2}$), whereas the death probabilities additionally decrease ($2.9 \times 10^{-5}$), and high nutrient availability extends further beyond the capillaries (see Fig. 7(b)).

### 3.2.1. Therapeutic outcomes

Initially, we considered tumors in which cells strongly compete for nutrients ($\beta = 0.1$). For a low endocytic rate ($\alpha_c = 1.0 \times 10^{-4}\,\mathrm{h}^{-1}$), even the most aggressive therapy (injected dose is equal to the maximum tolerated one, $C_0 = 0.6$ mM, administrated at each 4 h) can only reduce the tumor growth rate. In order to eradicate the tumor, a high endocytic rate ($\alpha_c = 5.0 \times 10^{-3}\,\mathrm{h}^{-1}$) combined with large therapeutic loads ($C_0 \geq 0.5$ mM) administrated at intervals $\tau = 4$ h is required. If the interval between successive doses is increased to 12 h, the tumor survives although shrunk to a few hundred cells along the therapy. These results are shown in Fig. 8(a). Finally, as expected, non-selective therapies exhibit similar outcomes but they are always slightly less efficacious.

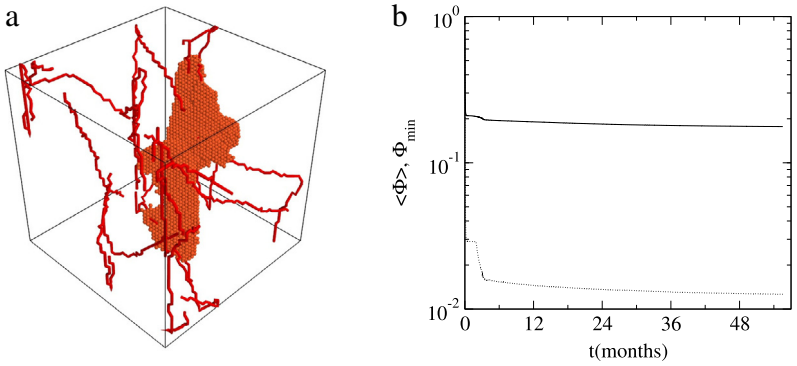


**Fig. 7.** (a) A low nutrient demanding tumor ($\beta = 0.08$) fed by the denser capillary network shown in Fig. 6(a) and (b) its nutrient spatial distribution at $z = L/2$ just before the therapy beginning. The tumor grew until it reaches the lattice borders.

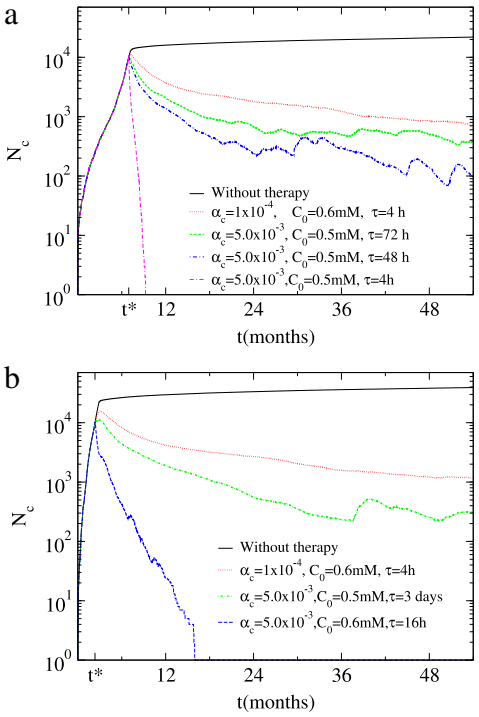


**Fig. 8.** Evolution in time of the number of cancer cells in highly vascularized tumors subjected to different therapeutic protocols (doses $C_0$, endocytic rates $\alpha_c$ and administration periods $\tau$) based on selective nanoparticles. The nutrient uptake rate by cancer cells is (a) $\beta = 0.1$ (high) and (b) $\beta = 0.08$ (low). Therapies begin at the time $t^*$.

In turn, for cancer cells consuming nutrients at a lower rate ($\beta = 0.08$), the tumor grows fast due to the larger nutrient supply available. In this case, the tumor cannot be eradicated if the nanoparticle endocytic rate is small ($\alpha_c = 1.0 \times 10^{-4}\ \mathrm{h}^{-1}$). Tumor eradication depends on larger endocytic rates ($\alpha_c = 5.0 \times 10^{-3}\ \mathrm{h}^{-1}$) and doses administrated at short intervals as, for instance, $C_0 = 0.6$ mM and $\tau = 16$ h. See Fig. 8(b). So, highly vascularized and fast growing tumors demand an extremely aggressive therapy to be eradicated. Although the dense capillary network feeding the tissue provides a high interstitial nanoparticle concentration, its value at the capillaries decays exponentially after drug administration. In contrast, the nutrient concentration is constant. Since both division and death probabilities of cancer cells depend on the free drug released within the cell and the local nutrient concentration, tumor eradication requires not only high CP–Dox doses administrated at short periods, but also a high endocytic rate of these nanoparticles.

Finally, we investigated the effect on therapeutic outcomes of partitioning the loads of nanoparticles and free doxorubicin under cell division. As previously mentioned, the model assumes that when a cancer cell undergoes mitosis, a fraction $\omega$ of both internalized nanoparticles and free drug within the cell are transferred to its daughter cell. Therapies based on perfectly selective nanoparticles ($\alpha_n = 0$) were simulated for either fixed values of $\omega$ ($\omega = 0, 0.1$ and $0.5$) or randomly chosen values at each cell division event. Our results for a tumor with $\beta = 0.08$, $C_0 = 0.6$ mM, $\alpha_c = 5.0 \times 10^{-3}\ \mathrm{h}^{-1}$, and $\tau = 24$ h are

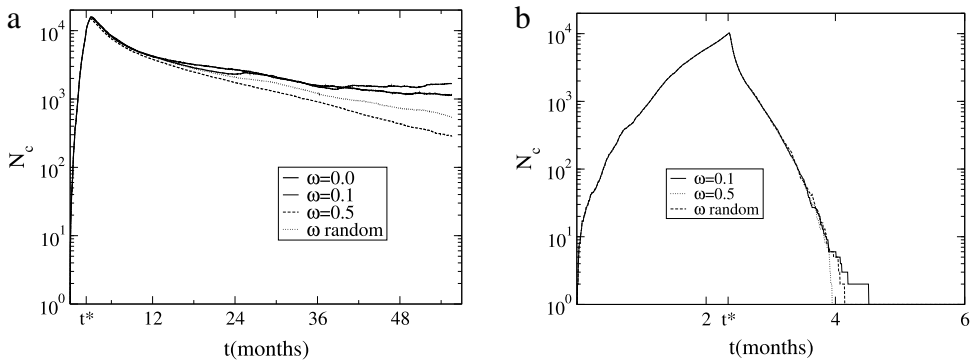


**Fig. 9.** Effect of CP–Dox and free drug transfer under cancer cell division for a therapy against a highly vascularized, fast growing tumor ($\beta = 0.08$). The therapeutic parameters are $C_0 = 0.6$ mM, $\tau = 24$ h, and $\alpha_n = 0$ (perfectly selective nanoparticles). The endocytic rate of nanoparticles is (a) $\alpha_c = 1 \times 10^{-4}$ and (b) $\alpha_c = 5 \times 10^{-3}$ h$^{-1}$.

shown in Fig. 9. The tumor is eradicated, no matter the value of $\omega$, and the curves for different values of $\omega$ are very similar. It is worth to mention that the major effect of drug partitioning is a small decrease in the time for tumor eradication. In summary, our results indicate that the CP–Dox nanoparticles and free Dox partitioning slightly increase the efficacy but are not determinant to the therapy's outcome.

## 4. Discussion

Considering the complexity and nonlinearities involved in cancer progression and its interaction with therapeutics, computational multiscale models are valuable tools to provide quantitative understanding of the major mechanisms controlling tumor–drug dynamics and to suggest how nanosized drug delivery systems should be engineered to enhance their therapeutic success. Here, we used a 3*D* multiscale model to evaluate the effects of tissue vascularization and nanotherapeutic's characteristics on tumor treatment outcomes.

We focused on an innovative and promising class of advanced drug carriers represented by the chimeric polypeptides that self-assemble into nanoparticles on doxorubicin attachment. Formulations using free doxorubicin exhibit serious side effects, as life-threatening heart problems and severe depletion of blood cells in the bone marrow, thereby strongly constraining their tolerated doses. Doxorubicin encapsulation within CP-nanoparticles partially overcomes this obstacle, leading to much higher tolerated doses of loaded nanoparticles. Furthermore, the nanoparticles exhibit good pharmacokinetics and tumor accumulation, low toxicity and high antitumoral efficacy [20].

The major results of our simulations are the following. The efficacy of nanochemotherapy is strongly dependent on tissue vascularization. Indeed, the eradication of tumors growing in highly vascularized tissues demands more aggressive therapies than those necessary for eradicating poorly vascularized tumors. The reason is that a dense capillary network ensures high interstitial concentrations of both nutrients and CP–Dox nanoparticles, but the drug concentration at the capillaries decays fast after its administration. Consequently, cell division will overcome cell death unless an aggressive therapy (high doses administered at short intervals) is applied. This find weakens the support for developing therapies that normalize the tumor vasculature [6–8]. Their rationale is appealing: fixing the vascular delivery system to both increase the total supplies and homogenize the distributions of drug and oxygen throughout the tumor. However, nutrients also become more available and distributed among cancer cells if the vascular normalization succeeds. A normalized tumor vascular network effectively works like the denser capillary systems considered in our computational model. But in this case, eradicating the tumor is harder. So, our simulations point to the opposite direction, namely, reduce the vasculature and impair its function. Since this is the goal of traditional antiangiogenic treatments, our find indicates the convenience of combining antiangiogenic and cytotoxic therapies.

It is worth to notice that here we modeled tumors similar to melanoma, which do not induce new vessel growth and primarily co-opt the existing capillary network for vascularization. For them there is no "delivery problem" beyond the diffusion limit. This view remains valid even considering angiogenesis that changes vessel morphology [11]. If vessel co-option and dematuration are taken into account, Alarcón et al. [19] showed that much larger regions populated by quiescent cells than those formed under normal vascularization are generated. In consequence, since quiescent cells are resistant to the cytotoxic drugs, the efficacy of the chemotherapy diminishes significantly. This result may explain the apparent success of combined vessel normalization therapy and chemotherapy. However, normalizing the tumor vasculature only produces transient and marginal gains in tumor's response to the cytotoxic drugs [19]. Our results suggest that even a permanent vascular normalization does not increase the therapeutic efficacy.

More relevant than tissue vascularization is the nanoparticle endocytic rate by cancer cells. If this endocytic rate is small, tumor eradication is impossible. The best therapeutic outcome is tumor remission and, afterwards, the control of its reduced size. In contrast, high endocytic rates can lead to tumor eradication. For densely vascularized tissues, large therapeutic loads administrated at very short intervals are required, whereas for poorly vascularized tissues it is possible

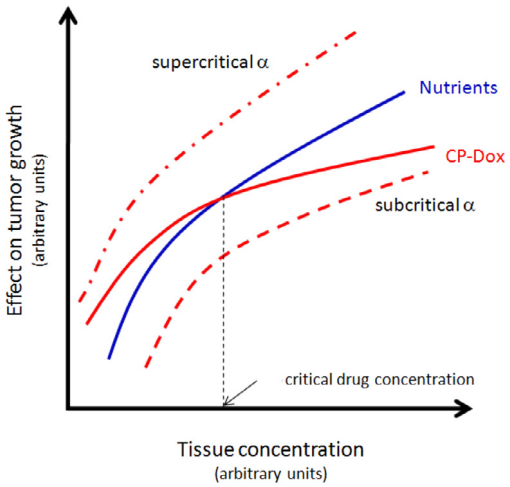


**Fig. 10.** Conceptual scenario for cancer nanochemotherapy. The relative strengths of nutrient and drug effects on tumor growth are represented on the vertical axis, and their amounts are on the horizontal axis. The nutrients enhance cancer cell proliferation and, in opposition, the drug impairs tumor growth, but the supply of both is regulated by the vascular network. The strength of drug inhibitory effect on cells is additionally and mainly determined by its endocytic rate. If the inhibitory effects overcome the proliferative ones, the tumor is eradicated. In the region of therapeutic success the curve for drugs lies above the curve for nutrients at least up to a critical concentration where these curves cross over. This "critical" point is primarily determined by the drug endocytic rate $\alpha$. For supercritical $\alpha$ the tumor will always be eradicated and there is no "critical point", while for subcritical $\alpha$ the tumor is never eradicated.

to combine large doses with longer delivery intervals or lower doses administered at shorter periods to eradicate the tumor. This flexibility can be exploited to generate a variety of safer and more efficacious therapeutic protocols. So, as for virus entry in oncolytic virotherapy [32,33], nanoparticle endocytic rate is the main feature to be enhanced in order to develop a successful cancer chemotherapy. This prominence is strengthened by the marginal influence of the other CP–Dox nanoparticle pharmacokinetic parameters. Indeed, our simulations indicate that increased nanoparticle selectivity for cancer cells or partitioning of encapsulated and free Dox under cancer cell division slightly increase the efficacy but are not determinant of the therapy's outcome.

Summarizing, our results support the simple conceptual scenario shown in Fig. 10. Tumor eradication depends on the balance between the nutrient supply and drug uptake by the cells, both regulated by the vascular network. Further, the drug's effect on cells is mainly determined by its endocytic rate. Hence, the tumor eradication or the control of its size demands either an anticancer drug with a very high endocytic rate (possibly unrealistic) or a combined therapy based on cytotoxic and antiangiogenic agents. Given a tumor type, which selects a nutrient response curve, and a specific cytotoxic nanomedicine, associated to a particular drug response curve, an adjuvant antiangiogenic therapy that reduces tumor vasculature, and thereby both drug and nutrient supplies to the cancer, triggers the system's sliding down along their response curves. Eventually, for a high but feasible endocytic rate, their crossing point is traversed and the combined therapy becomes successful. As a final remark, certainly monotonous response curves are oversimplified models for complex, multicellular processes affected by multiple factors which themselves dynamically change in space and time.

## 5. Conclusions

In the present work, a multiscale mathematical model integrating varied processes concerning tumor growth, CP–Dox pharmacokinetics and tissue vascularity was proposed and studied through computer simulations. The main aim was to evaluate tumor systemic response to nanochemotherapies. Our simulational results indicate that tumor eradication depends on the balance between the nutrient supply and drug uptake by the cells, both regulated by the vascular network. Further, the drug's effect on cells is mainly determined by its endocytic rate. Hence, the tumor eradication or the control of its size demands either an anticancer drug with a very high endocytic rate (possibly unrealistic) or a combined therapy based on cytotoxic and antiangiogenic agents. This main result fuels the debate on apparently disparate strategies to enhance cancer chemotherapy: combine cytotoxic therapies with either antiangiogenic agents or drugs that normalize the tumor vasculature. Since the eradication of tumors growing in highly vascularized tissues demands more aggressive therapies than those necessary for eradicating poorly vascularized tumors, our finds weaken the support to the latter strategy, currently under experimental test. Given the complexity of tumor–stroma interactions, mathematical modeling can help us to evaluate quantitatively these strategies or even the result of their combination. Thus, our theoretical results can shed light on the design of new protocols with neat potential impacts on the clinical practice.

## Acknowledgments

This work was partially supported by the Brazilian Agencies FAPEMIG (APQ-04232-10, APQ-02013-14 and PPM-00312-14); CNPq (306024/2013-6; 307182/2012-6 and 150879/2012-1) and CAPES (88881.030375/2013-1).

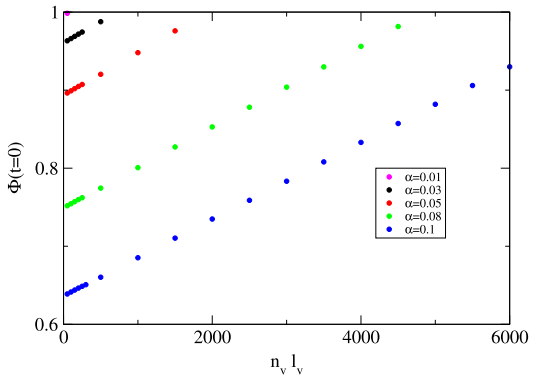


**Fig. A.11.** Mean stationary nutrient concentration at $t = 0$, $\Phi(t = 0)$, as a function of $n_v \times l_v$ (that corresponds to approximately the number of endothelial cells in the tissue) for different values of $\alpha$. At $t = 0$, the tissue is free from tumors except for a single cancer cell. The parameters $L = 50\Delta$ and $\lambda_\Phi = 10$ were fixed.

## Appendix A. The capillary network

The capillary network is defined in the normal tissue, before the introduction of the first cancer cell, and does not evolve in time. Capillaries average 8 μm in diameter [29], but for simplicity, in our model it is assumed that they occupy a lattice site ($\Delta \sim 20$ μm). Each vessel has approximately the same length, $l_v = 1$ mm [29], and grows accordingly a correlated random walk. Specifically, every vessel starts from randomly chosen sites on either the bottom or lateral lattice borders. The growth of each capillary begins along an initial direction, defined by the axial and azimuthal angles $\phi$ and $\theta$, chosen at random, and proceeds through successive steps of fixed length $\Delta$, the lattice constant. The direction of every step can deviate from that of the previous one by at most $\pm\delta\phi, \pm\delta\theta$, that control the vessel tortuosity. So, after $n$ steps, the direction of a capillary segment is given by $(\theta_n = \theta + \sum_{i=2}^{n} \xi_i, \phi_n = \phi + \sum_{i=2}^{n} \eta_i)$, with $\xi_i$ and $\eta_i$ randomly chosen in the ranges $[-\delta\theta, +\delta\theta]$ and $[-\delta\phi, +\delta\phi]$, respectively, $\forall i = 1, 2, \ldots$. The values $\delta\phi = 0.1$ and $\delta\theta = 0.2$ were used in the simulations. Also, if an advancing vessel eventually intercepts a previous one, its growth continues without interference, leading behind a joint connecting the two capillaries. Finally, if the vessel reaches one of the tissue borders, a new direction is chosen in order to allow its growth within the considered tissue section. It is assumed that all vessels have the same diameter, and the distinction between veins and arteries is neglected.

It is assumed that the nutrient concentration in the capillaries is constant along the blood vessels, and that it diffuses into the normal tissue and tumor. In Fig. A.11 it is shown the mean initial nutrient concentration versus $n_v l_v$ (approximately the total number of lattice sites belonging to the capillary network) for cancer cells consuming about $\lambda_\Phi = 10$ times more glucose than normal cells with varying uptake rates $\alpha$. Since these vessels are free from spatial and temporal heterogeneity in blood flow, this vasculature is functionally normal. However, its structure is abnormal because the capillaries are tortuous and have a random pattern of tissue coverage. So, our simple algorithm generates vasculatures spatially similar to those resulting from tumor angiogenesis [34,35].

## Appendix B. Simulation protocol and model parameters

Here, the simulation protocol and model parameter estimates are briefly described. Additional details are found in Refs. [21,23]. The simulations were implemented as follows. At each time step, Eq. (1) is numerically solved in the stationary state ($\partial N/\partial t = 0$) through relaxation methods. Also, Eq. (6) for CP–Dox diffusion throughout the tissue is iterated 1056 times taking into account the analytically known solution for its concentration at the capillary vessel, obtained from Eq. (5). Determining the CP–Dox concentration at the sites occupied by cells, the fraction of the drug internalized by the cells is calculated. Then, the intracellular load of free Dox is determined and the "cell viability" $V$ of each cell (normal and tumoral) is evaluated. Provided the nutrient concentration at any lattice site and the viability of every cell, $N$ cells are sequentially selected at random with equal probability. (Here, $N(t)$ is the total number of living cells at the time $t$.) For each one of them, a tentative action is randomly chosen with equal probability. These actions are division, death, or migration for a malignant cell and just death for a normal one. The selected cell action will be implemented or not according to the corresponding local probabilities determined by Eqs. (2)–(4), and the time is incremented by $\Delta t = 1/N(t)$. At the end of this sequence of $N(t)$ updates, a new time step begins and the entire procedure (solution of the nutrient diffusion equations, CP–Dox spreading and endocytosis, and application of the cell dynamics) is iterated.

In all simulations, the tissue is represented by a cubic lattice of linear size $L = 50\Delta$ and lattice constant $\Delta = 20$ μm, corresponding to a tissue volume of about 1 mm$^3$. Assuming a DNA synthesis phase of the cell cycle lasting about 11 h [36], one time step in the simulations corresponds to about 4–5 h. The parameters $\lambda_\Phi = 10$, $\theta^n_{die} = 0.001$, $\theta^c_{div} = 0.1$, and $\theta^c_{die} = 0.001$ were fixed and the glucose uptake rate $\beta'$ constrained within the range $[10^{-6}, 10^{-4}]$ s$^{-1}$ in order to generate compact tumor growth patterns. The chemotherapy begins when the tumors have $N_0 = 10{,}000$ cells.

**Table B.1**
Parameter values used for compact tumor morphologies ($\theta^n_{die} = \theta^c_{die} = 0.001$, and $\theta^c_{div} = 0.1$).

| Parameter | Description | Value |
|---|---|---|
| $D_N$ | Nutrient (glucose) diffusivity | $5^{-6}$ cm$^2$/s |
| $\beta'$ | Nutrient uptake rate of normal cells | $10^{-6}$–$10^{-4}$ s$^{-1}$ |
| $\lambda$ | Multiplicative factor in cancer cell's uptake | 10 |
| $\Delta$ | Linear cell size | 10 $\mu$m |
| $k_1$ | Drug's removal rate | 0.96 h$^{-1}$ |
| $k_2$ | Drug's accumulation rate in tissues | 0.80 h$^{-1}$ |
| $D$ | Drug's diffusivity | $2.64 \times 10^{-2}$ mm$^2$ h$^{-1}$ |
| $IC_{50}$ | Half maximal inhibitory concentration | 1.8 $\mu$M |

The glucose consumption rate for normal cells is $10^{-6}$ s$^{-1} < \beta' < 10^{-4}$ s$^{-1}$ [37] and the glucose diffusion constant for EMT6 tumor spheroids is $D_g = 5 \times 10^{-6}$ cm$^2$/s [37], thus leading to $\beta = \Delta\sqrt{\beta'/D_g}$ in the range $\beta \sim 10^{-3}$ to $10^{-2}$. In the simulations were used $\beta$ values up to two orders of magnitude greater.

The parameters characterizing the pharmacokinetics of CP–Dox nanoparticles were taken from Ref. [20]. So, the following drug's clearance rates $k_1 = k_{el} + (k_{pt} - k_{tp}) = 0.96$ h$^{-1}$ and $k_2 = k_{pt} - k_{tp} = 0.8$ h$^{-1}$ were used. These values result from the rates $k_{el} = 0.16$, $k_{pt} = 4.7$, and $k_{tp} = 3.9$ h$^{-1}$ reported in Ref. [20]. We assumed that the CP–Dox diffusivity is similar to those of viruses with comparable sizes. Hence, a diffusion coefficient $D = 2.64 \times 10^{-2}$ mm$^2$ h$^{-1}$ was used [22]. Finally, Mackay et al. have shown that $F = a\{1 - \exp[-(\ln 2)(t/t_{1/2})]\}$ is the fraction of intracellularly released Dox. For computational simplicity, a constant fraction $a = 0.68$, corresponding to their asymptotic value, was used in our simulations. This factor increments the intracellular free Dox concentration by $\Delta C_3(\vec{x}, t) = a\beta_{n,c}C_2(\vec{x}, t)$ at each time step.

Concerning the cytotoxic effect of CP–Dox, the assays performed in Ref. [20] give a cell viability $V = 1/[1 + (C_3/IC_{50})^p]$. In our simulations, the measured value $IC_{50} = 1.8$ $\mu$M was used. A value $p = 1$ was chosen. Table B.1 summarizes the model parameters and their values used in our simulations.

The remaining parameters, $C_0$, $\tau$, $\alpha_n$, and $\alpha_c$, key for determining the therapeutic outcome, were varied in the simulations. The values used were 200, 500, and 600 $\mu$M for $C_0$; 4, 12, 16, 24, 36, 48, 72, and 192 h for $\tau$; and $5 \times 10^{-3}$ and $1 \times 10^{-4}$ for $\alpha_{n,c}$. The magnitude of $\alpha$ deserves a brief comment. From the essays of Chithrani and Chan [38], it seems that cells endocytose about $10^3$ transferrin-coated gold nanoparticles of 50 nm in 6 h. Considering a cellular volume of 1 nanolitre, an extracellular nanoparticle concentration of 0.02 nM, and assuming that the molar concentration internalized per hour is given by $\Delta C_3 = \alpha_{n,c}C_2$, we find $\Delta C_3 \sim 0.3$ pM h$^{-1}$ and, consequently, $\alpha_{n,c} = \Delta C_3/C_2 \sim 10^{-2}$ h$^{-1}$.

## References


[1] A.Z. Wang, R. Langer, O.C. Farokhzad, Nanoparticle delivery of cancer drugs, Annu. Rev. Med. 63 (2012) 185–198.
[2] E. Blanco, A. Hsiao, A.P. Mann, M.G. Landry, F. Meric-Bernstam, M. Ferrari, Nanomedicine in cancer therapy: Innovative trends and prospects, Cancer Sci. 102 (2011) 1247–1252.
[3] K. Cho, X. Wang, S. Nie, Z. Chen, D.M. Shin, Therapeutic nanoparticles for drug delivery in cancer, Clin. Cancer Res. 14 (2008) 1310–1316.
[4] S.D. Perrault, C. Walkey, T. Jennings, H.C. Fischer, W.C.W. Chan, Mediating tumor targeting efficiency of nanoparticles through design, Nano Lett. 9 (5) (2009) 1909–1915.
[5] V.P. Chauhan, T. Stylianopoulos, Y. Boucher, R.K. Jain, Delivery of molecular and nanoscale medicine to tumors: transport barriers and strategies, Annu. Rev. Chem. Biomol. Eng. 2 (2011) 281–298.
[6] R.K. Jain, Normalization of tumor vasculature: An emerging concept in antiangiogenic therapy, Science 307 (5706) (2005) 58–62.
[7] R.K. Jain, Normalizing tumor microenvironment to treat cancer: bench to bedside to biomarkers, J. Clin. Oncol. 31 (17) (2013) 2205–2218.
[8] V.P. Chauhan, J.D. Martin, H. Liu, D.A. Lacorre, S.R. Jain, S.V. Kozin, T. Stylianopoulos, A.S. Mousa, X. Han, P. Adstamongkonkul, Z. Popović, P. Huang, M.G. Bawendi, Y. Boucher, R.K. Jain, Angiotensin inhibition enhances drug delivery and potentiates chemotherapy by decompressing tumour blood vessels, Nat. Commun. 4 (2013) 2516.
[9] M.R. Owen, T. Alarcón, P.K. Maini, H.M. Byrne, Angiogenesis and vascular remodelling in normal and cancerous tissues, J. Math. Biol. 58 (4–5) (2009) 689–721.
[10] A. Shirinifard, J.S. Gens, B.L. Zaitlen, N.J. Poplawski, M. Swat, J.A. Glazier, 3D multi-cell simulation of tumor growth and angiogenesis, PLoS One 4 (10) (2009) e7190. http://dx.doi.org/10.1371/journal.pone.0007190.
[11] M. Welter, K. Bartha, H. Rieger, Emergent vascular network inhomogeneities and resulting blood flow patterns in a growing tumor, J. Theoret. Biol. 250 (2) (2008) 257–280.
[12] J. Wu, Q. Long, S. Xu, A.R. Padhani, Study of tumor blood perfusion and its variation due to vascular normalization by anti-angiogenic therapy based on 3D angiogenic microvasculature, J. Biomech. 42 (6) (2009) 712–721.
[13] M. Wu, H.B. Frieboes, S.R. McDougall, M.A. Chaplain, V. Cristini, J. Lowengrub, The effect of interstitial pressure on tumor growth: coupling with the blood and lymphatic vascular systems, J. Theoret. Biol. 320 (2013) 131–151.
[14] E.J. Koay, M.J. Truty, V. Cristini, R.M. Thomas, R. Chen, D. Chatterjee, Y. Kang, P.R. Bhosale, E.P. Tamm, C.H. Crane, M. Javle, M.H. Katz, V.N. Gottumukkala, M.A. Rozner, H. Shen, J.E. Lee, H. Wang, Y. Chen, W. Plunkett, J.L. Abbruzzese, R.A. Wolff, G.R. Varadhachary, M. Ferrari, J.B. Fleming, Transport properties of pancreatic cancer describe gemcitabine delivery and response, J. Clin. Investig. 124 (2014) 1525–1536.
[15] J. Pascal, E.L. Bearer, Z. Wang, E.J. Koay, S.A. Curley, V. Cristini, Mechanistic patient-specific predictive correlation of tumor drug response with microenvironment and perfusion measurements, Proc. Natl. Acad. Sci. 110 (35) (2013) 14266–14271.
[16] H.B. Frieboes, M. Wu, J. Lowengrub, P. Decuzzi, V. Cristini, A computational model for predicting nanoparticle accumulation in tumor vasculature, PLoS One 8 (2) (2013) e56876. http://dx.doi.org/10.1371/journal.pone.0056876.
[17] J. Pascal, C.E. Ashley, Z. Wang, T.A. Brocato, J.D. Butner, E.C. Carnes, E.J. Koay, C.J. Brinker, V. Cristini, Mechanistic modeling identifies drug-uptake history as predictor of tumor drug resistance and nano-carrier-mediated response, ACS Nano 7 (12) (2013) 11174–11182.
[18] J. Sinek, S. Sanga, X. Zheng, H. Frieboes, M. Ferrari, V. Cristini, Predicting drug pharmacokinetics and effect in vascularized tumors using computer simulation, J. Math. Biol. 58 (4–5) (2009) 485–510.
[19] T. Alarcón, M.R. Owen, H.M. Byrne, P.K. Maini, Multiscale modelling of tumour growth and therapy: the influence of vessel normalisation on chemotherapy, Comput. Math. Methods Med. 7 (2–3) (2006) 85–119.

[20] J.A. MacKay, M. Chen, J.R. McDaniel, W. Liu, A.J. Simnick, A. Chilkoti, Self-assembling chimeric polypeptide–doxorubicin conjugate nanoparticles that abolish tumours after a single injection, Nature Mater. 8 (12) (2009) 993–999.
[21] S.C. Ferreira, M.L. Martins, M.J. Vilela, Reaction–diffusion model for the growth of avascular tumor, Phys. Rev. E 65 (2) (2002) 021907.
[22] L.R. Paiva, C. Binny, S.C. Ferreira, M.L. Martins, A multiscale mathematical model for oncolytic virotherapy, Cancer Res. 69 (3) (2009) 1205–1211.
[23] L.R. Paiva, M.L. Martins, A multiscale model to evaluate the efficacy of anticancer therapies based on chimeric polypeptide nanoparticles, Appl. Phys. Lett. 98 (5) (2011) 053703.
[24] M. Cross, H. Greenside, Pattern Formation and Dynamics in Nonequilibrium Systems, Cambridge University Press, Cambridge, UK, 2009.
[25] H.D. Summers, P. Rees, M.D. Holton, M.R. Brown, S.C. Chappell, P.J. Smith, R.J. Errington, Statistical analysis of nanoparticle dosing in a dynamic cellular system, Nat. Nanotechnol. 6 (3) (2011) 170–174.
[26] B. Döme, S. Paku, B. Somlai, J. Tímár, Vascularization of cutaneous melanoma involves vessel co-option and has clinical significance, J. Pathol. 197 (3) (2002) 355–362.
[27] B. Döme, M.J. Hendrix, S. Paku, J. Tóvári, J. Timar, Alternative vascularization mechanisms in cancer: Pathology and therapeutic implications, Amer. J. Pathol. 170 (1) (2007) 1–15.
[28] J.A. Kim, C. Åberg, A. Salvati, K.A. Dawson, Role of cell cycle on the cellular uptake and dilution of nanoparticles in a cell population, Nat. Nanotechnol. 7 (1) (2012) 62–68.
[29] R.A. Freitas, Nanomedicine, Volume I: Basic Capabilities, Landes Bioscience, Georgetown, TX, 1999.
[30] A. Hirayama, K. Kami, M. Sugimoto, M. Sugawara, N. Toki, H. Onozuka, T. Kinoshita, N. Saito, A. Ochiai, M. Tomita, H. Esumi, T. Soga, Quantitative metabolome profiling of colon and stomach cancer microenvironment by capillary electrophoresis time-of-flight mass spectrometry, Cancer Res. 69 (11) (2009) 4918–4925.
[31] Y. Urasaki, L. Heath, C.W. Xu, Coupling of glucose deprivation with impaired histone H2B monoubiquitination in tumors, PLoS One 7 (5) (2012) e36775.
[32] L.R. Paiva, M.L. Martins, S.C. Ferreira, Questing for an optimal, universal viral agent for oncolytic virotherapy, Phys. Rev. E 84 (4) (2011) 041918.
[33] L.R. Paiva, H.S. Silva, S.C. Ferreira, M.L. Martins, Multiscale model for the effects of adaptive immunity suppression on the viral therapy of cancer, Phys. Biol. 10 (2) (2013) 025005.
[34] B.J. Vakoc, R.M. Lanning, J.A. Tyrrell, T.P. Padera, L.A. Bartlett, T. Stylianopoulos, L.L. Munn, G.J. Tearney, D. Fukumura, R.K. Jain, et al., Three-dimensional microscopy of the tumor microenvironment in vivo using optical frequency domain imaging, Nat. Med. 15 (10) (2009) 1219–1223.
[35] Y.-A. Liu, S.-T. Pan, Y.-C. Hou, M.-Y. Shen, S.-J. Peng, S.-C. Tang, Y.-C. Chung, 3-d visualization and quantitation of microvessels in transparent human colorectal carcinoma, PLoS One 8 (11) (2013) e81857.
[36] D.A. Rew, G.D. Wilson, Cell production rates in human tissues and tumours and their significance. Part II: clinical data, Eur. J. Surg. Oncol. 26 (4) (2000) 405–417.
[37] K. Smallbone, R.A. Gatenby, R.J. Gillies, P.K. Maini, D.J. Gavaghan, Metabolic changes during carcinogenesis: potential impact on invasiveness, J. Theoret. Biol. 244 (4) (2007) 703–713.
[38] B.D. Chithrani, W.C.W. Chan, Elucidating the mechanism of cellular uptake and removal of protein-coated gold nanoparticles of different sizes and shapes, Nano Lett. 7 (6) (2007) 1542–1550.